Smart Mater. Struct. **15** (2006) 1–9 UNCORRECTED PROOF

Post-buckled precompressed piezoelectric flight control actuator design, development and demonstration

Ron Barrett[1,2], **Ross McMurtry**[1,3], **Roelof Vos**[1,2], **Paolo Tiso**[1] and **Roeland De Breuker**[1]

[1] Faculty of Aerospace Engineering, Technical University of Delft, Netherlands
[2] Aerospace Engineering Department, The University of Kansas, Lawrence, KS, USA
[3] Imperial College, London, UK

Received 20 June 2005, in final form 11 July 2006
Published
Online at stacks.iop.org/SMS/15/1

Abstract

This paper describes a new class of flight control actuators using post-buckled precompressed (PBP) piezoelectric elements. These actuators are designed to produce significantly higher deflection *and* force levels than conventional piezoelectric actuator elements. Classical laminate plate theory (CLPT) models are shown to work very well in capturing the behavior of the free, unloaded elements. A new high transverse deflection model which employs nonlinear structural relations is shown to successfully predict the performance of the PBP actuators as they are exposed to higher and higher levels of axial force, which induces post-buckling deflections. A proof-of-concept empennage assembly and actuator were fabricated using the principles of PBP actuation. A single grid-fin flight control effector was driven by a 3.5″ (88.9 mm) long piezoceramic bimorph PBP actuator. By using the PBP configuration, deflections were controllably magnified 4.5-fold with excellent correlation between theory and experiment. Quasi-static bench testing showed deflection levels in excess of ±6° at rates exceeding 15 Hz. The new solid state PBP actuator was shown to reduce the part count with respect to conventional servoactuators by an order of magnitude. Power consumption dropped from 24 W to 100 mW, weight was cut from 108 to 14 g, slop went from 1.6° to 0.02° and current draw went from 5 A to 1.4 mA. The result was that the XQ-138 subscale UAV family experienced nearly a 4% reduction in operating empty weight via the switch from conventional to PBP actuators, while in every other measure gross performance was significantly enhanced.

(Some figures in this article are in colour only in the electronic version)

Nomenclature

Symbol	Description	Units
a	Integrating factor	
A, B, D	In-plane, coupled, bending laminate stiffnesses	lb in^{-1}, lb, in lb (N m^{-1}, N, N m)
AR	PBP amplification ratio = $\delta(F_a > 0)/\delta(F_a = 0)$	
b	Actuator width	in (mm)
c	Integrating factor	
E	Stiffness	GPa (msi)
M	Applied moment vector	N m m^{-1} (in lb in^{-1})
N	Applied force vector	N m^{-1} (lb in−1)
t	Thickness	in (mm)
y	Out of plane displacement dimension	in (mm)
z	Through thickness dimension	in (mm)
α	Angle of attack	deg.
δ	PBP beam angle	deg.
δ_0	PBP end rotation angle	deg.
ε	Laminate in-plain strain	μstrain

κ	Laminate curvature	rad in^{-1} (rad m^{-1})
Λ	Piezoelectric free element strain	μstrain
σ	Stress	msi (GPa)
Subscripts		
a	Actuator	
b	Bond	
ex	External	
l	Laminate	
s	Substrate	
t	Thermally induced	

1. Introduction

For nearly 100 years, the fundamental properties of piezoelectric elements have been successfully modeled. Many different classes of actuators from sonar to stereo tweeters to helicopter rotor blade elements have been made using piezoelectric sheets, stacks and blocks as driving elements [1]. Numerous studies have been centered on the addition of various types of mechanisms, the use of different lamination techniques and/or shapes to amplify either deflection at the expense of force or force at the expense of deflection [2–7]. In each case some finite amount of total work was lost in the conversion process while weight, volume, complexity and cost penalties were incurred. Because many classes of aircraft have extremely tight weight, volume and performance requirements, they tend to drive actuators to smaller packages with higher levels of performance. Several other classes of piezoelectric actuators to be investigated as of late employ dynamic effects of oscillating piezoelectric, electrostrictive and/or magnetostrictive elements in linear- and rotary-inchworm type motors. Although well suited for some applications, their system-level power densities, bandwidths, form factors and costs are currently not compatible with some of the most demanding classes of aircraft.

Q.1

Among these most demanding types of aircraft are the small uninhabited aerial vehicles (UAVs), known as mini- or micro-aerial vehicles (MAVs). Similarly, guided hard-launched munitions also present similar challenges to the design engineer with bandwidths ranging in excess of 300 Hz at setback accelerations of upwards of 100 000 g. In recent years, these extreme requirements in bandwidth, weight, volume, environmental and deflection requirements have lead to the development of new, high performance actuators which are specifically tailored to these types of aircraft [8–10]. Figure 1 shows the first MAV which was enabled by piezoelectric Flexspar flight control actuators.

Although these actuators have been shown to work for many classes of aircraft, their performance could be improved still further. Although previously unpublished, it is well known by those who work with many of these classes of flight control actuators that deadband, slop and power density are often challenging issues for the design engineer to work around.

One of the most capable UAVs which has been developed to date is the XQ-138 [11]. The XQ-138 is designed to take off and land vertically, hover like a helicopter, then pitch over and transition to airplane-mode flight for dash out, cruise and loiter to speeds in excess of several hundred kts. Because this class of convertible UAVs is also intended to operate in urban and forested environments in any type of weather, the demands on the flight control assembly are extremely high. Accordingly, the purpose of this paper is to lay out a new class of actuator which is designed to significantly enhance the overall performance of the XQ-138 while decreasing actuator weight and volume fractions, thereby opening up total useful load.

Because nearly all actuator schemes which have employed piezoelectric actuators have been centered on various arrangements that trade force for stroke while degrading the total work available, a new approach is needed. In the late 1990s Lesieutre conceived a piezoelectric transformer which was designed with axially compressed piezoelectric elements [12]. The axial compression levels were close to the buckling load which effectively nulled some of the loss generating mechanism inherent in most piezoelectric actuator designs. References [12] and [13] showed that by doing this, the overall energy conversion efficiency of the entire system could be made higher than the efficiency of the raw material itself. Accordingly, this paper lays out several years of research which have been centered on improving and bringing this fundamental discovery to the aerospace flight control community [14, 15].

2. Analytical modeling

2.1. Generic actuator set-up

To take advantage of the principles laid out in references [12] and [13], a piezoelectric bender element is arranged in a pin–pin configuration with an externally applied axial force which is close to the perfect column buckling load. The axial force, F_a, is applied so that as the piezoelectric moment is applied a controlled 'imperfection' induces further, but controlled, deformation. The overall goal of this post-buckled precompressed (PBP) actuator assembly is to simultaneously and controllably amplify both the force and deflection levels

Figure 1. The Lutronix Kolibri, the world's first VTOL MAV enabled by piezoelectric flexspar stabilators (1997) [11].

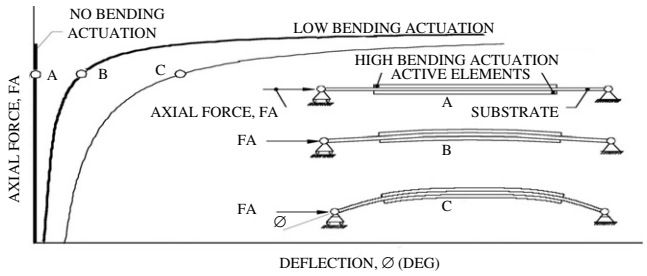

Figure 2. Generic arrangement of the post-buckled precompressed (PBP) actuator arrangement.

which can be generated by solid state piezoelectric bender elements. The addition of various forms of compliant mechanisms on either end of the actuator allows for a higher level of controllability, but generally retards the ultimate deflection levels so the size, weight and complexity of such mechanisms are typically minimized. Because essentially any level of deflection can be excited via the application of ever higher loads, great care is taken in the design as the external face of the convex actuator element will suffer from various forms of tensile failure including depoling and mechanical fracture if the bending levels are too high. Figure 2 shows the overall arrangement of the actuator including the pin–pin supports, axial force and generic end extensions.

The static behavior of the unloaded PBP bender element is easily captured by using classical laminated plate theory (CLPT) models. The bender is made from two primary components: a pair of piezoelectric actuator sheets bonded to a structurally stiff substrate. As the piezoelectric sheets are commanded to alternatively expand and contract, the bender element deflects up and down. An important aspect of the design involves the use of coefficient of thermal expansion (CTE) mismatch which has been used for more than 20 years to precompress tension-sensitive piezoceramic elements and pretension usually metallic isotropic substrates [7, 10]. The static, unloaded ($F_a = 0$) behavior of the device can be modeled easily by the techniques described in [1] and [16]. Assuming an unloaded structure and using CLPT methods, the following holds. The applied forces and moments may be balanced by stress distributions which are distributed through the thickness of the element:

$$N = \int \sigma \, \mathrm{d}z \qquad M = \int \sigma Z \, \mathrm{d}z. \tag{1}$$

Actuator in-plane forces and moments (a) can be expressed as a balance with external forces and moments (ex) and forces and moments due to mismatches in coefficients of thermal expansion (t). These factors will generate in-plane laminate strains, ε, and curvatures, κ.

$$\begin{Bmatrix} N \\ M \end{Bmatrix}_{\mathrm{ex}} + \begin{Bmatrix} N \\ M \end{Bmatrix}_{\mathrm{a}} + \begin{Bmatrix} N \\ M \end{Bmatrix}_{t} = \begin{bmatrix} A & B \\ B & D \end{bmatrix}_1 \begin{Bmatrix} \varepsilon \\ \kappa \end{Bmatrix}. \tag{2}$$

If the external forces and moments are ignored and thermally induced stresses are not considered, equation (2) can be reduced to

$$\begin{bmatrix} A & B \\ B & D \end{bmatrix}_l \begin{Bmatrix} \varepsilon \\ \kappa \end{Bmatrix} = \begin{bmatrix} A & B \\ B & D \end{bmatrix}_{\mathrm{a}} \begin{Bmatrix} \Lambda \\ 0 \end{Bmatrix}. \tag{3}$$

At this point, equation (3) can be easily solved for laminate curvature, κ, by assuming that a balanced, symmetric laminate composed of isotropic or quasi-isotropic elements are used:

$$\kappa = \frac{B_{\mathrm{a}}}{D_l}\Lambda. \tag{4}$$

By using the unloaded laminate curvature, κ, as a starting point, the problem can now be defined in terms of gross curvatures with externally applied axial force, F_a, as follows.

Figure 3 shows that the length along the surface of the element, s, and the length along the major axis of the element, x, are related by the curvature induced in the actuator. The angular coordinate, δ, is maximized at the ends of the element, δ_0, and goes to zero at the mid-point.

One can consider the normal strain of any point in the PBP actuator at a distance y from the neutral axis through its thickness as

$$\varepsilon = \frac{y \, \mathrm{d}\delta}{\mathrm{d}s} = \frac{\sigma}{E}. \tag{5}$$

If one examines the individual beam element and assumes pure bending, then the following holds:

$$\sigma = \frac{My}{I}. \tag{6}$$

Accordingly, combining equations (5) and (6) with CLPT conventions and terminology, equation (7) is obtained:

$$\frac{y \, \mathrm{d}\delta}{\mathrm{d}s} = \frac{My}{Db}. \tag{7}$$

Because the externally applied moment loading in each section comes from the axial force, F_a,

$$M = -F_{\mathrm{a}} y. \tag{8}$$

Substituting equation (8) into (7) yields

$$\frac{\mathrm{d}\delta}{\mathrm{d}s} = -\frac{F_{\mathrm{a}} y}{Db}. \tag{9}$$

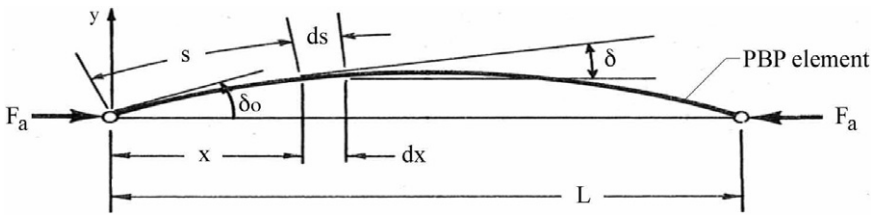

Figure 3. Analysis terms and conventions for analysis of the PBP actuator arrangement.

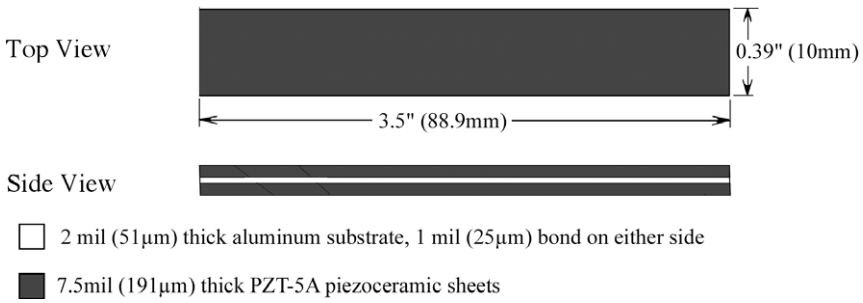

Figure 4. PBP grid fin actuator geometry.

Differentiating equation (9) with respect to s,

$$\frac{\mathrm{d}^2\delta}{\mathrm{d}s^2} = -\frac{F_\mathrm{a}}{Db}\sin\delta. \tag{10}$$

Multiplying through by the integrating factor $2\frac{\mathrm{d}\delta}{\mathrm{d}s}$,

$$2\frac{\mathrm{d}\delta}{\mathrm{d}s}\frac{\mathrm{d}^2\delta}{\mathrm{d}s^2} = -2\frac{F_\mathrm{a}}{Db}\sin\delta\frac{\mathrm{d}\delta}{\mathrm{d}s}. \tag{11}$$

Integrating equation (11) yields

$$\left(\frac{\mathrm{d}\delta}{\mathrm{d}s}\right)^2 = 2\frac{F_\mathrm{a}}{Db}\cos\delta + a. \tag{12}$$

If one considers the addition of an applied moment via piezoelectric elements as generating an imperfection across the beam, then the unknown integrating factor, a, can be solved for, given that at $x = 0$, $\delta = \delta_0$, $\frac{\mathrm{d}\delta}{\mathrm{d}s} = \kappa$.

$$\left(\frac{\mathrm{d}\delta}{\mathrm{d}s}\right)^2 = 2\frac{F_\mathrm{a}}{Db}(\cos\delta - \cos\delta_0) + \kappa^2. \tag{13}$$

With appropriate trigonometric substitutions and considering the negative root because $\mathrm{d}\delta$ is always negative,

$$\frac{\mathrm{d}\delta}{\mathrm{d}s} = -2\sqrt{\frac{F_\mathrm{a}}{Db}}\sqrt{\mathrm{Sin}^2\left(\frac{\delta_0}{2}\right) - \mathrm{Sin}^2(\delta/2) + \frac{\kappa^2 Db}{4F_\mathrm{a}}}. \tag{14}$$

For solution, a change of variable is as follows:

$$\mathrm{Sin}\,(\delta/2) = c\sin\xi \tag{15}$$

where ξ is a variable with the value $\pi/2$ when $x = 0$ and the value 0 when $x = L/2$. Accordingly, when $x = 0$,

$$c = \mathrm{Sin}\left(\frac{\delta_0}{2}\right). \tag{16}$$

Solving for δ and differentiating yields

$$\begin{aligned}\delta &= 2\sin^{-1}\left(\mathrm{Sin}\left(\frac{\delta_0}{2}\right)\sin\xi\right)\\ \mathrm{d}\delta &= \frac{2\mathrm{Sin}\left(\frac{\delta_0}{2}\right)\cos\xi}{\sqrt{1-\mathrm{Sin}^2\left(\frac{\delta_0}{2}\right)\sin^2\xi}}\,\mathrm{d}\xi.\end{aligned} \tag{17}$$

Combining equations (14) through (17) with appropriate end values,

$$\begin{aligned}\sqrt{\frac{F_\mathrm{a}}{Db}}\int_0^{1/2}\mathrm{d}s &= \frac{L}{2}\sqrt{\frac{F_\mathrm{a}}{Db}}\\ &= \int_0^{\pi/2}\frac{\mathrm{Sin}\left(\frac{\delta_0}{2}\right)\cos\xi}{\left(\sqrt{\mathrm{Sin}^2\left(\frac{\delta_0}{2}\right)\cos^2\xi + \frac{\kappa^2 Db}{4F_\mathrm{a}}}\right)\left(\sqrt{1-\mathrm{Sin}^2\left(\frac{\delta_0}{2}\right)\sin^2\xi}\right)}\,\mathrm{d}\xi.\end{aligned} \tag{18}$$

3. Actuator design and fabrication

3.1. Overall design

The actuator element was designed to generate deflections and maintain moment and bandwidth capabilities suitable for controlling the XQ-138 MAV. Toward that end, a PBP actuator element of the following geometry was laid out:

The grid fins which are employed on the XQ-138 family of MAVs are multicellular and provide pitch and yaw control to the aircraft. They have been designed to possess very low pitching moments about the pivot point and yet provide very high normal force gradients with deflection. These properties allow the aircraft to maintain stable flight in very gusty conditions and excellent levels of control authority throughout all flight regimes from hover, through transition and high speed airplane-mode flight. Figure 5 shows the grid-fins integrated on the lower fuselage of the aircraft.

To demonstrate the PBP actuator, a truncated fuselage demonstration rig was designed. This rig employed a sectioned lower fuselage and bearing assembly supporting a fully flightworthy grid fin equipped empennage.

3.2. PBP grid fin actuator test article fabrication

Prior to integration in a flightworthy aircraft, an experimental test rig was fabricated and tested. This rig employed all of the salient features of a flightworthy empennage, except that only one grid fin was used rather than a complete set of four and the fuselage tube was opened and truncated so that all components might be observed during operation. Figure 6 shows the layout of the test rig.

The graphite–epoxy structures were fabricated from Cyanimide 123 pre-impregnated graphite cloth while the PBP actuator element was laid up in a 250 °F (121 °C) high temperature cure so as to precompress the piezoceramic elements. The axial force bands were made from silicone

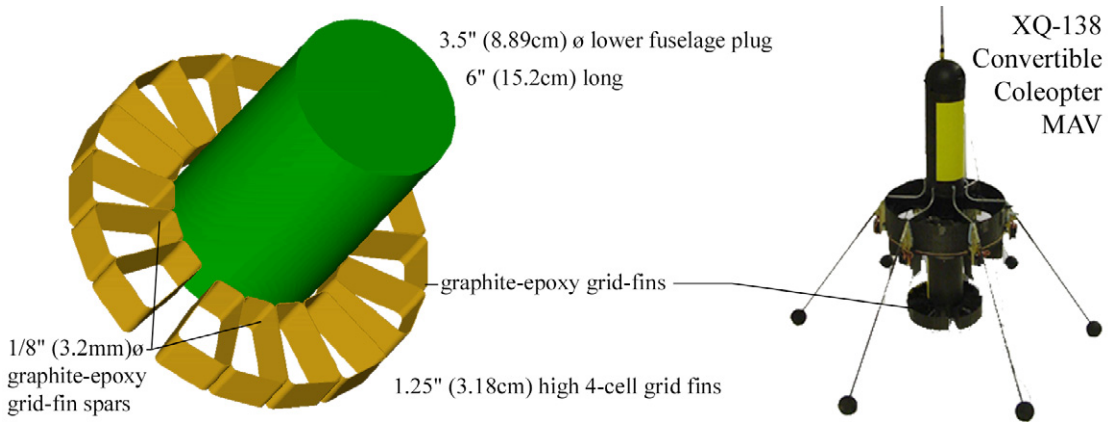

Figure 5. Graphite-epoxy grid fin assembly on lower fuselage of XQ-138 MAV.

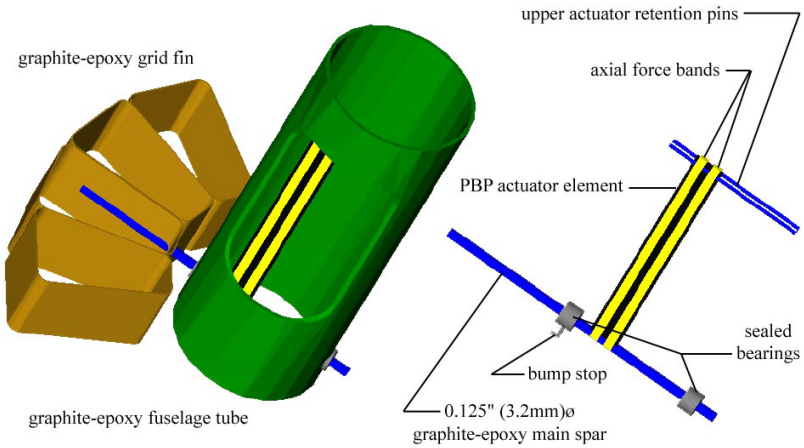

Figure 6. Grid fin test rig assembly with integral PBP actuator and structural mounts.

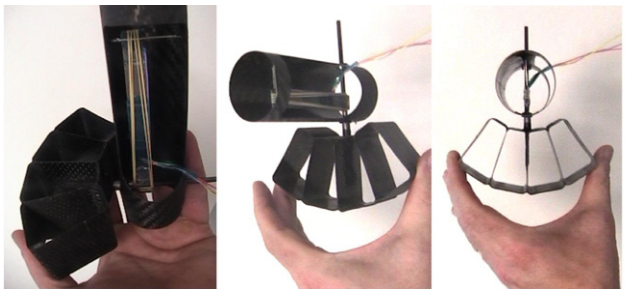

Figure 7. Grid-fin test rig assembly prior to mounting on the seismic base.

elastic material and provided a scheduled amount of axial force so as to induce post-buckled behavior as seen in figure 2.

4. Experimental testing and results

4.1. Quasi-static bench testing

A series of experiments was conducted on the actuator assembly so as to verify the analytical models of section 2 and demonstrate the working principles of the actuator. Laser reflection techniques were used to measure grid fin angular deflections to 0.01° of accuracy. Figure 7 shows the grid fin test rig assembly prior to mounting in the seismic test base.

The first set of tests was conducted quasi-statically with driving signals being fed to the test apparatus at 1 Hz. A sweep of voltage and axial force was made so as to determine just how expanded the design envelope can become. Figure 8 shows the deflection, δ_0, as a function of applied voltage and axial force. It should be noted that the bump stops were set at $\pm 7°$ so that tensile depoling and mechanical failure of the piezoceramic actuator elements could be avoided.

Of course, it is important for the overall benefit of the PBP system to be tracked in terms of total level of deflection amplification. Figure 9 shows the deflection trends with and without application of axial force, F_a, via the axial force bands.

From figures 8 and 9, it can be seen that the PBP analysis techniques presented in section 2 underpredicted the amount of deflection by up to 10%. It is suspected that creep effects induced such disparity between theory and experiment as the difference between the two trend lines grew as the period was increased from 1 s. It should also be noted that the amplification ratio between the conventional bender line ($F_a = 0$) and the measured PBP deflections is relatively steady at approximately AR = 4.5.

4.2. Dynamic bench testing

A series of dynamic bench tests was conducted to determine the frequency response of the actuator. Laser reflection techniques were used to determine performance. The fin

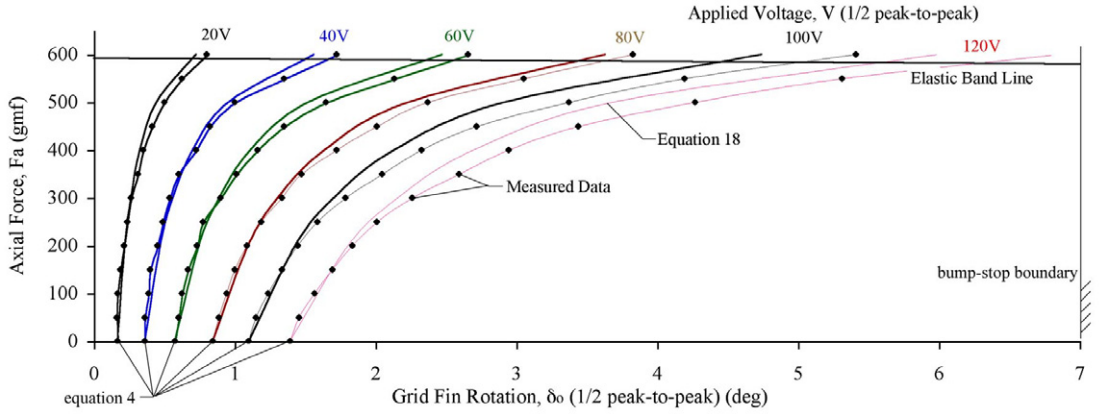

Figure 8. Correlation of grid fin deflection angle, δ_0, applied voltage and axial force, F_a.

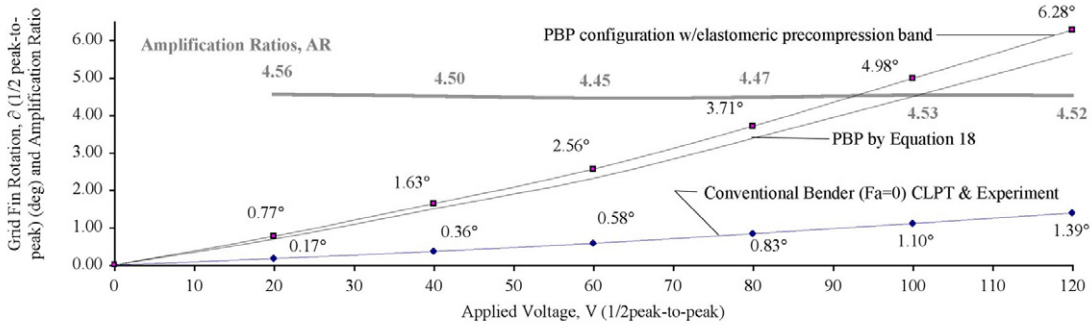

Figure 9. Performance comparison of PBP and conventional actuator elements.

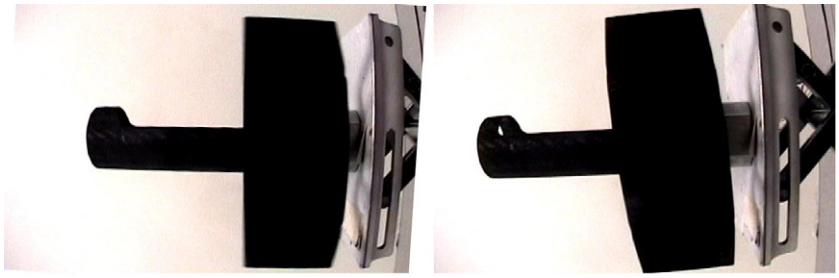

Figure 10. Grid fin test article mounted on seismic base unactuated and undergoing dynamic deflections.

assembly was mounted to a seismic test rig as shown in figure 10.

Because actuator bandwidth is so important to aircraft flight control systems, the following Bode amplitude plots were obtained for both the unamplified version of the actuator ($F_a = 0$) and the PBP configuration with the elastic band in place.

From figure 11 it can be seen that the dynamic performance is degraded as the level of axial force is increased from 0 to just under 1.32 lb (600 gmf, 5.87 N), with resonance peaks moving from 18 to 15 Hz. However, given the performance of conventional flight control servoactuators, this is still far superior to those that are typically available on the open market and those originally used on the XQ-138.

4.3. Wind tunnel testing

A series of wind tunnel tests were conducted to ensure that no flutter or divergence tendencies were present and that deflections remain steady with airspeed. Wind tunnel testing was conducted in the Auburn University 3 in × 4 in (91 cm × 122 cm) subsonic wind tunnel at speeds up to 120 ft s^{-1} (71 kts, 82 mph, 36.5 m s^{-1}). Figure 12 shows that the deflections are neither amplified nor degraded with increased airflow up through the test speeds. Because the aerodynamic center, center of gravity and center of pressure are all aligned with the hinge line of the grid fins, adverse pitch deflections and flutter tendencies are effectively nulled as seen in figure 12.

4.4. Flight testing

Following successful wind tunnel tests, a complete empennage assembly was fabricated and flown on an autonomous variant of the XQ-138. The PBP empennage assembly weighed substantially less than its conventional electromagnetic servoactuator driven counterpart. Figure 13 shows the empennage assembly prior to integration into the aircraft.

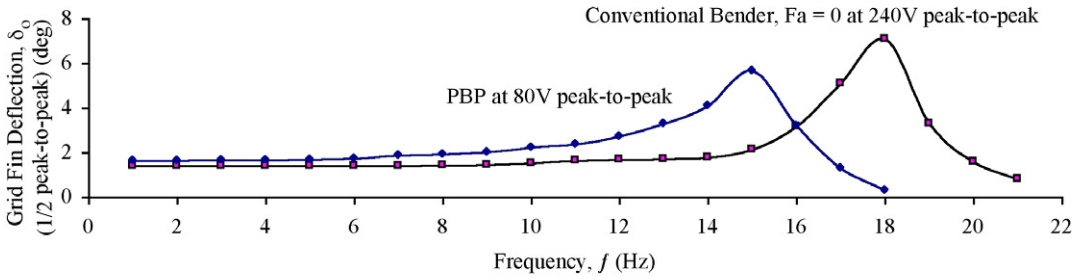

Figure 11. Dynamic performance of conventional bender and PBP variants of the grid fin actuator assembly.

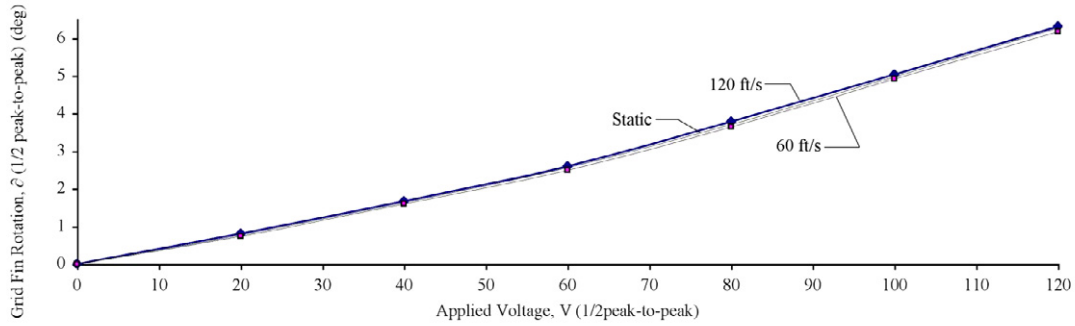

Figure 12. Grid fin performance in wind tunnel up to 120 ft s^{-1} (71 kts, 36.5 m s^{-1}).

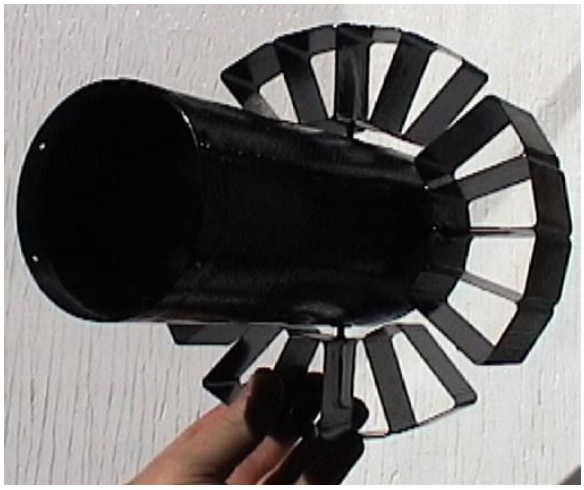

Figure 13. PBP grid fin assembly prior to integration into the flightworthy fully autonomous XQ-138 variant.

Flight testing confirmed that control authority of the conventional empennage was matched while responsiveness was increased nearly threefold. The substantial weight reduction in the empennage induced such a significant shift in center of gravity that components in the nose of the XQ-138 needed to be rearranged so as to maintain appropriate weight and balance. Figure 14 shows the modified variant of the XQ-138 in flight. More than 300 flight tests were performed on the aircraft, at facilities including Redstone Arsenal, AL, and Eglin AFB, FL. These flight tests demonstrated the need for high control authority mechanisms like grid fins combined with a long control arm distance from the c.g. so as to maintain both stability and control in adverse wind conditions. Although some of the flight tests were conducted in conditions as extreme as ±40 kt gusting winds in more than 2″ h^{-1} of rain, the aircraft performed flawlessly and not a single aircraft was damaged, lost or experienced excessive flight path deviations in both hover mode and airplane mode flight.

4.5. Integration characteristics and comparison

Significant benefits are clearly obtained by switching from conventional electromagnetic servoactuators to PBP actuators. Figure 15 shows the weight savings in terms of aircraft operating empty weight (OWE) fraction. Because the PBP actuators have no push rods, linkages or heavy motors with windings, they are significantly lighter than conventional electromechanical servoactuators. Because PBP actuators operate with high voltage rather than high current, the weight of the leads was reduced dramatically and servoactuator generated EMI was essentially eliminated (an important characteristic in such tight confines as an aircraft fuselage). Their low power consumption also induced a shrinkage in the size of the power supply systems on board the aircraft which further aided in boosting mission performance. Unlike conventional servoactuators, the PBP actuator is solid state so the part count, slop and deadband levels are one to two orders of magnitude below conventional servoactuators as seen in table 1.

Power consumption was measured at the maximum deflections at the maximum frequency for both classes of actuators. From table 1, it can be seen that both the current and total power consumption levels of the PBP class actuators are significantly lower than conventional actuators. Because

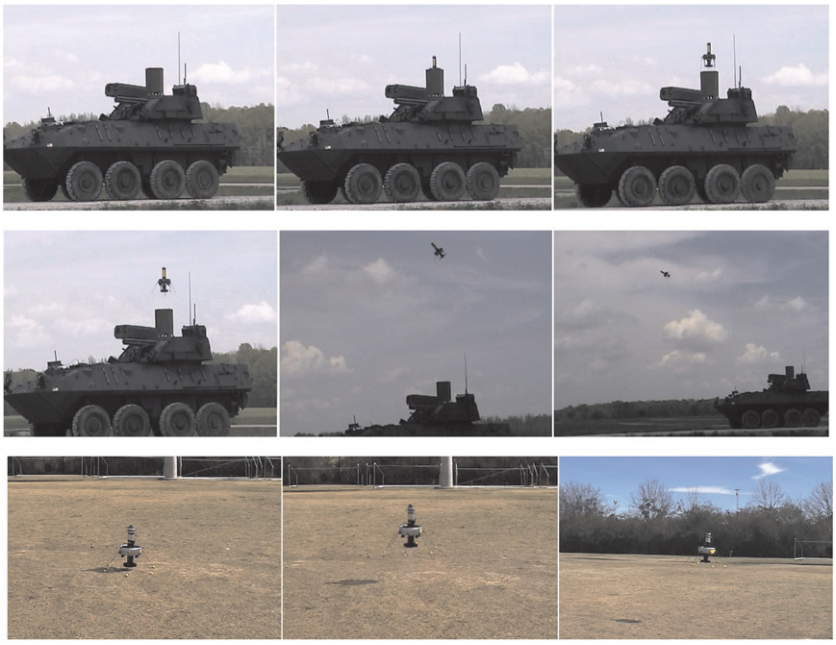

Figure 14. XQ-138 with PBP grid-fin empennage during flight testing at US Army Redstone Arsenal, AL, from the future combat system (FCS) technology demonstrator, flying and landing autonomously.

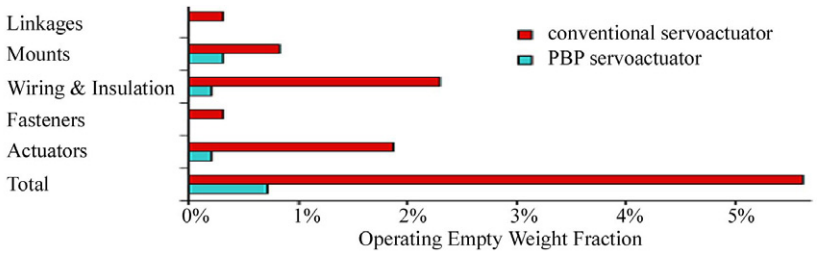

Figure 15. Comparison of PBP and conventional servoactuator operating empty weight fractions for the XQ-138.

Table 1. Comparison of PBP and conventional electromechanical pitch and yaw flight control actuator systems.

	Conventional servoactuator	PBP actuator
Max power	24 W	100 mW
Max current	5 A	1.4 mA
Mass	108 g	14 g
Slop	1.6°	0.02°
Break frequency	3 Hz	21 Hz
Part count	56	6

the measured deadband and slop was reduced by two orders of magnitude, the tendency to be susceptible to buffet vibrations is also essentially eliminated. Finally, the great simplicity of the PBP system is seen in a part count reduction which will ultimately help keep manufacturing costs low.

5. Conclusions

It can be concluded that a new class of actuators employing axial forces to induce post-buckled deflection amplification possesses significant benefits over conventional piezoelectric and electromechanical servoactuators. Classical laminated plate theory models are shown to accurately capture the performance of the actuators with no axial force. A new model designed to capture the large deformation behavior of post-buckled precompressed actuators is shown to work very well. A series of piezoelectric specimens were built to demonstrate the utility of the new post-buckled precompressed (PBP) actuator scheme. These actuator elements were designed as actuators for grid fins for a new class of subscale UAVs, in particular the XQ-138 convertible coleopter. An extensive series of tests with varying levels of axial precompression showed that static deflections could be controllably magnified approximately 4.5-fold over conventional levels, with excellent agreement between theory and experiment. The prototype flight control actuators were designed to nominally generate flight control deflections up to $\pm 5^\circ$ at rates in excess of 15 Hz. Because the PBP actuators are much simpler and operate as highly efficient solid state actuators, they consume 0.4% of the power, weigh 87% less, move seven times faster and possess an order of magnitude fewer parts than conventional servoactuators. Because they do not employ any linkages or pushrods, their slop levels are reduced by more than 98%. The result of these benefits is that the operating empty weights of the XQ-138 family are enhanced by nearly 4% while gross performance is improved in every other measure. Q.3

Acknowledgments

The authors would like to acknowledge the outstanding contributions of the many students and colleagues who helped with this study, including Mr Christoph Burger, Professor Eelco Jansen, Mr Koen Artois, Professor R Steven Gross and Mr Bill Holbrook. This study was sponsored by the AAL and the Faculty of Aerospace Engineering of the Technical University of Delft, Netherlands.

References

[1] Crawley E F and De Luis J 1987 Use of piezoelectric actuators as elements of intelligent structures *AIAA J.* **25** 987–97

[2] Prechtl E F and Hall S R 1999 Design of a high efficiency, large stroke electromechanical actuator *J. Smart Mater. Struct.* **8** 13–30

[3] Moskalik A J and Brei D 1998 Analytical dynamic performance modeling for individual c-block actuators *J. Vib. Acoust.* **121** 221–30

[4] Moskalik A J and Brei D 1999 Force-deflection behavior of piezoelectric c-block actuator arrays *Smart Mater. Struct.* **8** 531–43

[5] Ervin J and Brei D 1998 Recurve piezoelectric-strain-amplifying actuator architecture *IEEE/ASME Trans. Mechatron.* **3** 293–301

[6] Clement J, Brei D, Moskalik A and Barrett R 1998 Bench-top performance characterization of a c-block driven active flap system *Proc. 39th Structures Structural Dynamics and Mater. Conf. (Long Beach, CA, April 1998)* (Washington, DC: American Institute of Aeronautics and Astronautics) paper no. AIAA-98-2039

[7] Schwartz R W, Laoratanakul P, Nothwang W D, Ballato J, Moon Y and Jackson A 2000 Understanding mechanics and stress effects in rainbow and thunder actuators *SPIE Smart Struct. Mater. Active Mater.: Behavior and Mechanics* **3992** 363

[8] Barrett R, Burger C and Melian J P 2001 Recent advances in uninhabited aerial vehicle (UAV) flight control with adaptive aerostructures *Proc. 4th Euro. Demonstrators Conf. (Edinburgh, Scotland, Dec. 2001)*

[9] Barrett R and Lee G 2000 Design criteria, aircraft design, fabrication and testing of sub-canopy and urban micro-aerial vehicles *Proc. AIAA/AHS Int. Powered Lift Conf. (Alexandria, VA, Nov. 2000)*

[10] Barrett R and Stutts J 1998 Development of a piezoceramic flight control surface actuator for highly compressed munitions *Proc. 39th Structures, Structural Dynamics and Materials Conf. (Long Beach, CA, April 1998)* (Washington, DC: American Institute of Aeronautics and Astronautics) paper no. AIAA-98-2034

[11] Barrett R 2004 Adaptive aerostructures, improving high performance, subcale military UAVs *45th AIAA/ASME/ASCE/AHS/ASC Structures, Structural Dynamics and Materials Conf., 12th AIAA/ASME/AHS Adaptive Structures Conf. (April 2004)* (Palm Springs, CA: AIAA) paper no. 2004-1886

[12] Lesieutre G A and Davis C L 1997 Can a coupling coefficient of a piezoelectric actuator be higher than those of its active material? *J. Intell. Mater. Syst. Struct.* **8** 859–67

[13] Lesieutre G A and Davis C L 2001 Transfer having a coupling coefficient higher than its active material *US Patent Specification* 6,236,143

[14] Barrett R M and Tiso P 2005 Post buckled precompressed actuator *International Patent Application* PCT/NL2005/000054, by the Technical University of Delft, Holland

[15] Barrett R M, McMurtry R, Vos R, Tiso P and De Breuker R 2005 Post-buckled precompressed (PBP) elements: a new class of flight control actuators enhancing high-speed autonomous VTOL MAVs SPIE Paper No. 5762-16 *Society of Photo-Optical Instrumentation Engineers (SPIE) Annual Int. Symp. on Smart Structures and Materials (San Diego, CA, March 2005)*

[16] Jones R M 1975 Micromechanical behavior of a lamina *Mechanics of Composite Materials* (New York: Hemisphere Publishing Corporation)

Queries for IOP paper 228442

Journal: **SMS**
Author: **R Barrett et al**
Short title: **PBP piezoelectric flight control actuator design, development and demonstration**

Page 2

Query 1:-

Author: Please be aware that the colour figures in this proof will normally only appear in colour in the online Web version. If you require colour in the printed journal and have not previously arranged it, please contact the Publishing Administrator now.

Page 4

Query 2:-

Author: Figure 4 is not cited in text.

Page 8

Query 3:-

Author: We have followed the pdf version of figure 14. OK?